JOURNAL OF CHEMICAL & ENGINEERING DATA

Article

pubs.acs.org/jced

Interfacial Tension of (Brines + CO_2): (0.864 NaCl + 0.136 KCl) at Temperatures between (298 and 448) K, Pressures between (2 and 50) MPa, and Total Molalities of (1 to 5) mol·kg^{-1}

Xuesong Li, Edo Boek, Geoffrey C. Maitland, and J. P. Martin Trusler*

Qatar Carbonates and Carbon Storage Research Centre (QCCSRC), Department of Chemical Engineering, Imperial College London, South Kensington Campus, London SW7 2AZ, United Kingdom

ABSTRACT: We report the interfacial tension between carbon dioxide and aqueous solutions of the mixed salt system (0.864 NaCl + 0.136 KCl) with total salt molalities between (0.98 and 4.95) mol·kg^{-1}. The measurements were made at temperatures between (298 and 473) K at various pressures up to 50 MPa by means of imaging a pendant drop of CO_2-saturated brine surrounded by a water-saturated CO_2 phase. The expanded uncertainties at 95 % confidence are 0.05 K in temperature, 70 kPa in pressure, and for interfacial tension γ, the larger of 0.016γ and 0.6 mN·m^{-1}. The results of the study indicate that the interfacial tension increases linearly with the molality of the salt solution. An empirical equation has been developed to represent the present results as a function of temperature, pressure, and molality with an expanded uncertainty of 1.6 mN·m^{-1}.

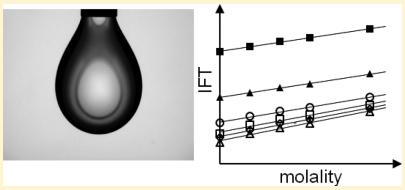

INTRODUCTION

Oil reservoirs are porous rocks containing oil and gas at high temperatures and pressures deep underground. After primary and secondary production, at least 50 % of the original oil in place (OOIP) is left behind in the reservoir.[1] Interfacial tension (IFT) is considered to be an important factor that may render 30 % of the OOIP unrecoverable by solution gas drive or water flooding alone. Improved recovery may be obtained by injecting carbon dioxide to displace and dissolve some of the remaining oil.[2] In general, it has been found that such a tertiary processes can enhance oil recovery by (8 to 16) % of the OOIP.[3] Interfacial phenomena between hydrocarbon-, water-, and CO_2-rich phases clearly play a very important role in determining the effectiveness of CO_2-enhanced oil recovery (CO_2-EOR).

In the CO_2-EOR processes, both of the relative permeabilities of the formation to oil and CO_2 and the residual oil saturation can be related to the oil-CO_2 and brine-CO_2 interfacial tensions through a dimensionless number which compares either the capillary and viscous forces in horizontal displacement processes or the capillary and buoyancy forces in gravity drainage processes.[4−6] Although there have been some studies of the effects of IFT in oil-CO_2 and water-CO_2 systems on the relative permeabilities in the CO_2 flooding process,[7−11] there are insufficient data available in the literature for analyzing the effects of IFT among oil, CO_2, and brine on the CO_2-EOR process. It has been found that the viscosity of an oil−brine system is significantly reduced when CO_2 is injected into an oil reservoir at a high reservoir pressure.[12,13] The reduced interfacial tension alters the viscous force-capillary force balance and thus lowers the residual oil saturation. Finally, the low viscosity of supercritical CO_2 puts severe limits on the efficiency of both carbon storage and CO_2-EOR as the sweep efficiency is often reduced due to channelling and fingering effects, associated with reservoir heterogeneity.[14] Therefore, it is of fundamental and practical importance to study the detailed effects of the viscous and capillary forces on various CO_2 flooding processes.

Carbon dioxide capture and storage (CCS) has the potential to significantly reduce CO_2 emissions to atmosphere from power generation and some other industrial processes. The general idea of CCS is to capture CO_2 from large point sources, such as fossil fuel power plants, fuel processing, and other industrial plants, compress it, and then inject it into a suitable underground storage site. Possible locations for such geological sequestration include deep saline aquifers, unmineable coal seams, and depleted oil or gas reservoirs. Among these sequestration sites, deep offshore saline aquifers are considered to be the most promising option for long-term safe storage.[15] Studies by the Intergovernmental Panel on Climate Change (IPCC) and others indicate that CCS can decrease the CO_2 emissions to atmosphere from a typical coal-burning power plant by up to 90 %,[16] making the development of this technology an attractive prospect. The technologies and practices that have been developed for CO_2-EOR have to some extent applicability in carbon storage processes.

An examination of the literature shows that the IFT of (CO_2 + water) has been measured at pressures up to 60 MPa and temperatures up to 383 K,[17−20] and various factors affecting the accuracy of the measurements have been discussed by Georgiadis et al.[20] However, the IFT between CO_2 and brine at high temperatures and pressures has been studied by only a few authors. Bachu et al.[18,21] and Yang et al.[22] have measured the IFT of CO_2 against synthetic formation brines,

Received: October 9, 2011
Accepted: February 15, 2012
Published: March 1, 2012

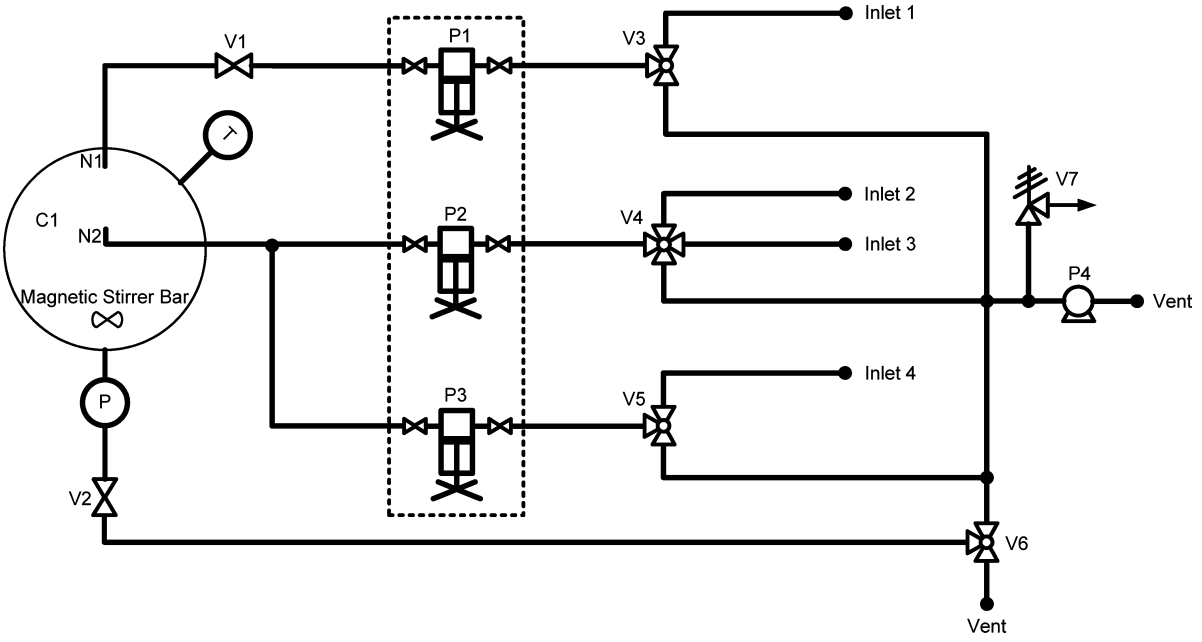

Figure 1. Schematic diagram of the apparatus: C1: windowed autoclave cell with stirrer; P1, P2, P3: high-pressure Quizix pump; T: temperature sensor (Pt100); P: flow-through pressure sensor (DF2): V1, V2: high-pressure valve (type 2); V3, V5, V6: three-way valve; V4: four-way switch; V7: relief valve; P4: vacuum pump; N1, N2: injection port.

having salinities of up to 334 010 $mg \cdot L^{-1}$, at temperatures T up to 398 K, and pressures $p \leq 27$ MPa. Their results show that IFT increases with increasing salinity and decreasing pressure, but a complex dependence of IFT on temperature was found. Aggelopoulos et al.[23,24] have performed IFT measurements for CO_2 with brines containing NaCl and/or $CaCl_2$ at $p \leq 25$ MPa at temperatures of (300, 344, and 373) K with a total salt molality of (0.09 to 3.0) $mol \cdot kg^{-1}$. They concluded that, at constant temperature and pressure, the IFT increases linearly with the molality of each salt present in the brine. Chalbaud et al.[17,25] reported IFT measurements between CO_2 and NaCl(aq) with pressures up to 25 MPa and temperatures up to 393 K. In contrast with the results of other authors, the IFT data of Chalbaud et al. show a different dependence on pressure: initially decreasing with increasing pressure but then reaching a plateau. However, these results also indicated a linear relationship between IFT and salt concentration when the other conditions are invariant.

To summarize the literature, measurements of IFT between brine and CO_2 under conditions of elevated pressure have been carried out on only a few different salt solutions. The available data are scattered and in some cases contradictory. Thus we conclude that additional high accuracy measurements would be useful to clarify the situation.

The object of this research is to investigate the dependence of IFT on temperature, pressure, and salinity (including both salt type and concentration) over the range of conditions applicable to CO_2 storage in underground reservoirs. One objective is to arrive at a universal model, based on such experimental evidence, for calculating the IFT of any (CO_2 + brine) system.

In this paper, we describe a new apparatus for carrying out the IFT measurements on corrosive fluids at high temperatures (up to 473 K) and high pressures (up to 50 MPa), and we report measurements for one brine system. The brine system studied in this work is $[(1 - y)$ NaCl + y KCl](aq), where y is the mole fraction of KCl in the salt; this was fixed at 0.136 in this work and is equivalent to a mass fraction of 0.2. This mixture is somewhat similar to some natural reservoir brines. The total salt molality of the investigated mixtures was between (0.98 and 4.95) $mol \cdot kg^{-1}$.

EXPERIMENT

High-Pressure Apparatus. Various techniques can be used to determine the interfacial tension between fluid phases. However, the pendant drop method is especially suitable for measuring IFT at high temperature and elevated pressures and has been used by some of us in previous work.[20] The IFT is determined from this method from images of a pendant drop by means of axisymmetric drop-shape analysis (ADSA).

The new apparatus, shown schematically in Figure 1, was designed and built in this work for the purposes of both IFT and contact angle measurements involving brines, CO_2, and hydrocarbons. All wetted metallic parts are made from either Hastelloy C276 or titanium, both of which are fairly resistant to corrosion in concentrated brines. The core of the apparatus is an autoclave view cell, indicated as C1 in the figure. This cell comprised a hollow cylindrical body, fabricated from Hastelloy C276, closed at either end by Hastelloy and sapphire window assemblies sealed with PTFE o-rings. The vessel was orientated with its axis horizontal, and the internal dimensions were: diameter 28 mm, length 40 mm. Four threaded fluid ports were machined in the body suitable for connection of 6.35 mm outer diameter (o.d.) coned-and-threaded high-pressure tubing. In the present work, reducing unions were fitted to two of these ports to permit connection of 1.6 mm o.d. tubing for fluid injection (N1 and N2); the third was connected to a tee union and thence to both a rupture-disk safety device and the drain valve, and the fourth port was plugged. The two reducing unions were drilled through so that the inlet capillaries (N1 and N2 in Figure 1) could pass to the interior of the cell such that drops or bubbles formed at the ends could be imaged. Pendant drops were formed from the end of capillary N1, which entered

dx.doi.org/10.1021/je201062r | J. Chem. Eng. Data 2012, 57, 1078–1088

through the top of the cell, while sessile drops or bubbles could be created from the tip of capillary N2.

A blind axial hole drilled in the vessel wall (5 mm diameter × 50 mm long) accommodated a Pt100 sensor that was used to measure the experimental temperature. To achieve a uniform temperature, the cell was enclosed in a five-piece close-fitting aluminum-alloy heater shell insulated on the outside by a jacket of silicone-rubber foam. Four cartridge heaters and an additional Pt100 temperature sensor were accommodated in axial holes bored in the heater shell, and used in conjunction with a PID process controller to regulate the temperature.

A supporting bracket was used to mount the cell horizontally on a 1 m long optical rail. Also mounted on the rail were an adjustable light-emitting diode (LED) light source, a diffuser, and a monochrome charge-coupled device (CCD) camera (IEEE1394 Digital FireWire camera, Foculus) fitted with a fixed focal length lens. Mixing of the cell contents was accomplished by means of an internal poly(tetrafluoroethylene) (PTFE)-coated magnetic stirrer bar (10 mm long × 3 mm diameter), driven by an external SmCo magnet assembly mounted on a shaft that passed through a small hole on the optical rail to a variable-speed electric motor beneath.

A flow-through pressure transducer (DJ Instruments, model DF2) was connected in the outlet line before valve V2 (see Figure 1). A system of three high-pressure syringe pumps (Quizix Q5000 series, Chandler Engineering) with wetted parts of Hastelloy C276 was used for injection of CO_2, brine, and wash water. Each syringe had a capacity of 10 mL and was fitted with its own safety head, pressure transducer, and air-actuated fill and dispense valves (not shown in Figure 1). To minimize dead volumes, 1.6 mm o.d. × 0.5 mm i.d. tubing (Hastelloy HC276) was used on all of the fluid connections between the pumps and the view cell. Referring to Figure 1, pump P1 was used for the brine, which was drawn in from the supply bottle through a filter with a 10 μm pore size. Pump P2 was used for flushing with pure water and, occasionally, other solvents and was provided with two alternative inlet lines also fitted with 10 μm pore-size filters. Finally, pump P3 was used for CO_2 injection. To permit charging of P3 with liquefied CO_2, the syringe was operated at a temperature of 283 K by passing water from a chiller unit through a jacket. A 0.5 μm pore size particulate filter was fitted in the CO_2 filling line. Valve V1 permitted isolation of the inlet capillary from P1, while valve V2 was used to control the fluid outlet; valve V6 was provided to permit connection of the outlet line to either a waste receiver or to a vacuum pump, the latter being protected from accidental overpressure by relief valve V7.

As implemented, the apparatus allowed the IFT to be measured at temperatures up to 473 K with pressures up to 50 MPa. Leaks are major concerns in this type of system. The system was therefore thoroughly leak-tested over the whole pressure range with both helium and water and exhibited a high-level of integrity.

Data Analysis. The ASDS technique is based on matching the shape profile of the drop with the theoretical profile obtained by numerical integration of the Young−Laplace equation. Referring to the lengths and angles defined in Figure 2, the theoretical profile may be obtained by the solution of the equation

$$\frac{d\theta}{dS} = 2 - \beta Y - \frac{\sin\theta}{X} \tag{1}$$

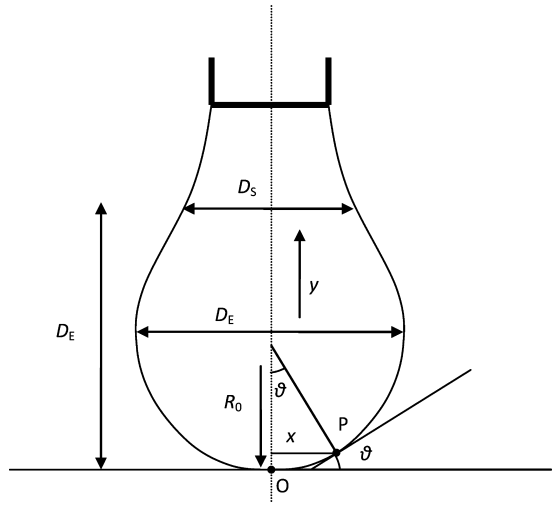

Figure 2. Profile of a pendant drop showing the coordinates used in the text. R_0 is the radius of curvature at the apex O, while s is the arc length between O and the point P; and y and x are respectively the vertical and horizontal coordinates relative to an origin at O.

together with the relations

$$\frac{dX}{dS} = \cos\theta \tag{2}$$

and

$$\frac{dY}{dS} = \sin\theta \tag{3}$$

where $X = x/R_0$, $Y = y/R_0$, $S = s/R_0$ are dimensionless coordinates of a point P on the profile of the drop, R_0 is the radius of curvature at the apex of the drop, and β is a dimensionless shape parameter related to the interfacial tension by

$$\gamma = \Delta\rho g R_0^2/\beta \tag{4}$$

Here, $\Delta\rho$ is the density difference between the drop and the surrounding medium, and g is the gravitational acceleration. In the analysis, the task is to find by trial or otherwise the values of R_0 and β that best match the experimental drop profile; then subject to a given value of $\Delta\rho$ the interfacial tension γ is obtained from eq 4.

In this research, commercial software (Advanced DROP-image, Ramé-Hart Instrument Co.) was used to perform the above procedure. The numerical methods used have been described in two papers by Hansen[25,26] and make use of the ratio $\sigma = D_S/D_E$ first introduced by Fordham[27] in 1938 for the purposes of obtaining initial estimates of β and R_0 from an experimental drop profile. The final values of these parameter are obtained by a fast optimization method involving a 3 × 3 matrix of drop profiles generated from eqs 1 to 3 for values of β and R_0 around the initial estimates. The Kutta-Merson[28] numerical integration algorithm is used with automatic step length adjustment.

Calibration. The Pt100 thermometer inserted in the body of the high pressure cell was calibrated at the temperature of the triple point of water and at four further temperatures in the range (323 to 473) K by comparison in a constant-temperature bath with a standard platinum resistance thermometer having an expanded uncertainty of 2 mK. Taking sensor drift and fluctuations of the thermostat into account, we estimate that

the overall expanded uncertainty of the cell temperature measurements was 0.05 K, with a coverage factor $k = 2$.

The model DF2 flow-through pressure transducer was calibrated against a hydraulic pressure balance (DH-Budenberg model 580EHX) having an expanded relative uncertainty of 0.008 % at six pressures up to 50 MPa. The mean and maximum absolute deviations arising from nonlinearity and hysteresis were (18 and 47) kPa, respectively. However, this sensor did drift over time, and corrections were required. The ambient pressure reading was compared and corrected before every experiment. Any difference was applied as a constant offset to correct subsequent readings in that run. Taking all factors into account, the expanded uncertainty of the pressure in the cell was estimated to be 70 kPa ($k = 2$).

Since the dimension R_0 appears in eq 1, it was necessary to calibrate the imaging system against a standard. This was done at the beginning of the experiment and every time after adjusting the lens on the camera. For this purpose, a calibration tool having a ball and a pin both of (4.000 ± 0.001) mm diameter (Precision Combo Calibration Device) was used. Typical drop sizes, quantified by $R_0 \approx 0.5D_E$, were approximately 2 mm, while an effective resolution of ± 0.5 pixels corresponded to ± 0.006 mm in the image. Thus the fractional resolution in the determination of R_0 is estimated to be approximately 0.3 %. Hansen[25,26] reports that, through the benefits of averaging, the effective resolution in edge recognitions can be better than ± 0.2 pixels.

Materials. Pure deionized and degassed water (electrical resistivity >18 MΩ·cm) was used. Carbon dioxide was supplied by BOC with a specific minimum mole fraction purity of 0.99995 in a cylinder fitted with a dip tube to permit withdrawal of liquid. Sodium chloride and potassium chloride were purchased from Sigma-Aldrich, with mass fraction purities of ≥ 0.995 and ≥ 0.99 %, respectively. Both salts were dried in an oven at $T = 373.15$ K. Solutions were prepared gravimetrically with the relative uncertainties in mass being below 0.01 %. Thus the relative uncertainty of molality was most probably limited only by the purity of the salts and was taken to be approximately 0.5 %. The brines were degassed by sonicating in an ultrasonic bath for 15 min immediately prior to use.

To calculate the IFT with the pendant drop method, the difference between the densities of the two fluids needs to be known. Since the two phases have very limited mutual solubility, this difference in densities is expected to be close to the difference between the densities of the pure brine and CO_2 at the temperature and pressure in question. However, at low temperatures and high pressures, where $\Delta\rho$ is small, errors in the phase densities have a large influence on the derived values of interfacial tension. Thus, in the absence of directly measured densities, the estimation of $\Delta\rho$ must be carried out carefully. The densities of coexisting phases in the (water + CO_2) system have been measured by Hebach et al.[29] at pressures up to 30 MPa and at temperatures between (284 and 322) K. They found that the density of the CO_2-rich phase did not differ from that of pure CO_2 within the experimental uncertainty of 0.15 %. The density of the aqueous phase was found to exceed that of pure water by an amount that follows the solubility of CO_2 in water, increasing with increasing pressure and declining with increasing temperature. For example, interpolated to $T = 298.15$ K, the lowest temperature in the present study, the density exceeds that of pure water by 16 kg·m^{-3} at $p = 30$ MPa. When the mass fraction w of dissolved CO_2 is evaluated from the model of Duan et al.,[30] the results of Hebach et al.[29] conform within experimental uncertainty to the simple model of Pruess and Spycher:[31]

$$1/\rho = (1 - w)/\rho_w + w/\rho^*_{CO_2} \quad (5)$$

Here, ρ_w is the density of water (or brine), and $\rho^*_{CO_2}$ is the inverse of the partial specific volume of CO_2 in solution, which is taken to be 1260 kg·m^{-3} independent of temperature and pressure. Since the model of Duan et al.[30] is also applicable to CO_2 solubility in brines, we have applied this with eq 5 and the same value of $\rho^*_{CO_2}$ to obtain the density of the aqueous phase. The density of the pure brine was obtained from measurements made in our laboratory which have a relative standard uncertainty of 0.015 %.[32] In view of the findings of Hebach et al.,[29] we take the density of the CO_2-rich phase to be that of pure CO_2, which we obtained from the equation of state of Span and Wagner.[33] Clearly, our method of estimating $\Delta\rho$ is subject to uncertainty most probably dominated by the effect of CO_2 dissolution on the density of the aqueous phase. For purposes of estimating the uncertainty of γ, we take the uncertainty $\delta(\Delta\rho)$ in the density difference to be one tenth of the difference between the calculated density of the CO_2-saturated brine and the density of the CO_2-free brine: $\delta(\Delta\rho) = 0.1(\rho - \rho_w)$. We note that the recalculation of γ is straightforward if more reliable experimental values of the density differences were to become available.

Experimental Procedure. Using the new apparatus, the IFT could be measured by imaging either a sessile CO_2 bubble injected through needle N2, in a CO_2-saturated bulk brine phase, or a pendant brine drop injected through needle N1 into a water-saturated CO_2 bulk phase. In theory, both approaches will present the same IFT value after the system reaches equilibrium. In view of the fact that pendant drops tend to be more stable than sessile bubbles, we opted for the second approach in this work. In practice, it was our experience that the brine drop, having a volume of less than 30 μL, injected into the 25 mL bulk phase required not more than about 10 min to be saturated with CO_2. To be sure that the CO_2 bulk phase was water-saturated, we first injected a few milliliters of brine into the bottom of the cell and stirred the system for at least 5 min.

Prior to first use, the entire system was cleaned very carefully with hexane, acetone, water, and CO_2 in sequence, repeated many times. Since a stable pressure is faster to achieve than a stable temperature, each group of IFT measurements was carried out at fixed temperature with rising pressures. Before measuring a new isotherm, the previously evacuated cell was first flushed several times with CO_2 and subsequently filled with CO_2 to a pressure of around 3 MPa, before closing the outlet valve of the CO_2 syringe pump and setting the desired operating temperature. After temperature stabilization, degassed brine was first compressed in pump P1 to a pressure slightly higher than that of the fluid in the cell, and then valve V1 was opened and a quantity of brine was pumped into the cell. The pressure of the cell was subsequently adjusted by discharging or injecting CO_2. Before measuring a new drop, at least three drops, together accounting for the dead volume downstream of valve V2, were discarded to ensure that every measured drop was independent and identically fresh when the measurement started. Once the measuring drop was formed at the end of needle N1, valve V1 was closed immediately, and drop imaging was started.

To ensure that the CO_2 was saturated with water, sufficient brine to fill the lower 1/8th of the cell was injected. The mixing device was turned on after every pressure change, as this greatly reduced the time required for rebalancing the system, but it was then turned off for the measurement.

The changes in the refractive index of the CO_2-rich bulk phase, arising from changes in pressure or temperature, had a marked influence on the focusing of the camera which was readjusted whenever the thermodynamic condition changed. The intensity of the light and the aperture of the lens were also adjusted to achieve satisfactory contrast and depth of field.

For every state point, at least three drops were measured, and each was monitored for at least 600 s with an interval of 6 s. As discussed in ref 20. the value of γ is expected to vary with time following the creation of a fresh drop. An initial variation with time should occur as CO_2 dissolves in the brine and eventually saturates the entire volume of the drop. The time scale for this is expected to be of the order of 1 min. Following this initial equilibration, the measured γ is expected to be essentially constant for an extended period, but on a much longer time scale, drift is expected as trace impurities diffuse toward the interface. This behavior was indeed observed, but the time dependence of γ differed with changes in temperature and pressure. At lower temperatures and high pressures, γ was observed to decrease rapidly in an initial transition period after the creation of each drop, as reported by many authors.[17,20,34−36] However, the same phenomenon was not obvious at high temperatures or at low pressures, presumably because diffusion coefficients increase rapidly with temperature while the CO_2 solubility declines with increasing temperature or reducing pressure. The time evolution of the measured IFT between CO_2 and (0.864 NaCl + 0.136 KCl)(aq) with molality m = 1.97 mol·kg^{-1} is shown in Figure 3 for different pressures

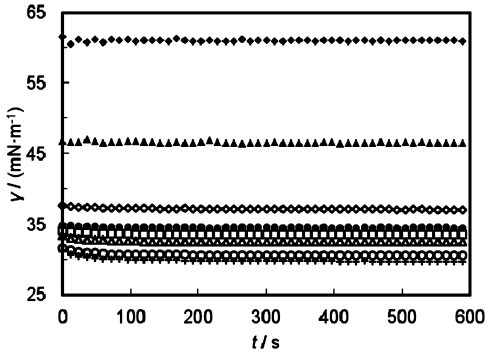

Figure 3. Interfacial tension of (0.864 NaCl + 0.136 KCl)(aq), m = 1.98 mol·kg^{-1}, as a function of time at different pressures, at T = 323.15 K: ◆, p = 2 MPa; ▲, p = 6 MPa; ◇, p = 10 MPa; ●, p = 16 MPa; □, p = 20 MPa; △, p = 30 MPa; ○, p = 40 MPa; +, p = 50 MPa.

at T = 323.15 K. The figure indicates that, at the same temperature, the time dependence is different at different pressures and that a steady value was achieved after about 150 s. This time became shorter with increasing temperature. The reported values of γ were therefore based on a mean computed over the period between (150 and 600) s after the creation of a fresh drop; the standard deviation was also computed.

Validation. The pendant drop method is well-established, and so just a few initial experiments were performed for validation purposes. The IFT of (air + H_2O) was measured at T = 298.15 K and ambient pressure. The interfacial tension was found to be (71.9 ± 0.1) mN·m^{-1}, in close agreement with the published value of Pallas and Harrison,[37] (71.99 ± 0.05) mN·m^{-1}. Additional confidence comes from comparing our results, extrapolated to zero molality, with the data for (CO_2 + water) reported previously[20] as discussed below.

RESULTS AND DISCUSSION

The IFT was measured for CO_2 and (0.864 NaCl + 0.136 KCl)(aq) for total salt molalities m, temperatures T, and pressures p as detailed in Table 1. The mole fractions of NaCl and KCl of

Table 1. Total Salt Molalities m, Temperatures T, and Pressures p Studied in This Work

m	T	p
mol·kg^{-1}	K	MPa
0.98	298, 323, 343, 373, 423, 448	2, 4, 6, 8, 10, 12, 14, 16, 18, 20, 25, 30, 35, 40, 45, 50
1.98	323, 343, 373, 393, 423	
2.97	298, 323, 343, 373, 393, 423	
4.95	323, 343, 373, 423	

the salt correspond to a mass ratio of 5:1, and total salinities up to 4.95 mol·kg^{-1} were studied. At least four isotherms were measured at each concentration. For each isotherm, 16 pressure points were measured from (2 to 50) MPa. The experimental data, 336 in number, are given in Tables 2 to 5. The relative standard deviation $\sigma(\gamma)/\gamma$ of the IFT data gathered at each state point was computed; on average it was 0.7 %. The overall relative standard uncertainty u_r of γ was calculated from the relation

$$u_r^2 = \left[\frac{1}{\gamma}\left(\frac{\partial\gamma}{\partial T}\right)_{p,m}\delta T\right]^2 + \left[\frac{1}{\gamma}\left(\frac{\partial\gamma}{\partial p}\right)_{T,m}\delta p\right]^2 + \left[\frac{1}{\gamma}\left(\frac{\partial\gamma}{\partial m}\right)_{p,T}\delta m\right]^2 + \left[\frac{\delta\Delta\rho}{\Delta\rho}\right]^2 + \left[\frac{\sigma(\gamma)}{\gamma}\right]^2 \quad (6)$$

and, except for a few points identified in Tables 1 to 3, it is given by the larger of 0.008γ and 0.3 mN·m^{-1}, leading to an expanded uncertainty at 95 % confidence equal to the larger of 0.016γ and 0.6 mN·m^{-1}. Four exceptional points are found at low temperature, low salt molality, and high pressure where the solubility of CO_2 in the brine is larger leading to increased uncertainty in $\Delta\rho$.

Figure 4 shows a comparison at T = 373 K between the interfacial tension of the CO_2 + (0.864 NaCl + 0.136 KCl)(aq) system studied in this work at m = 1.98 mol·kg^{-1} and values for the system CO_2 + NaCl(aq) from two different authors: Bachu and Bennion[18] at m = 2.15 mol·kg^{-1}, and Chalbaud et al.[17] at m = 1.79 mol·kg^{-1}. Assuming that the influence of Na^+ and K^+ ions on the interfacial tension are very similar, the results are comparable, and one would expect those of Chalbaud et al.,[17] (smaller m) to fall slightly lower, and those of Bachu and Bennion[18] (larger m) above, our data.

Variation with Pressure and Temperature. At all brine concentrations, γ is observed to decrease with increasing pressure when the salinity and the temperature are kept constant. The results for m = 1.98 mol·kg^{-1} are taken as an example and plotted in Figure 5. On each isotherm, it can been

Table 2. Interfacial Tension γ for CO_2 + (0.864 NaCl + 0.136 KCl)(aq) at Temperatures T, Pressures p, and Total Salt Molality m = 0.98 mol·kg^{-1} [a]

T	p	$\Delta\rho$	γ	T	p	$\Delta\rho$	γ
K	MPa	kg·m^{-3}	mN·m^{-1}	K	MPa	kg·m^{-3}	mN·m^{-1}
298.15	2	1008.0	55.3	373.15	2	971.7	55.4
298.15	4	955.4	43.9	373.15	4	941.1	51.0
298.15	6	859.1	32.4	373.15	6	906.1	46.8
298.15	8	274.1	28.8	373.15	8	866.2	43.1
298.15	10	234.3	27.7	373.15	10	820.4	39.7
298.15	12	207.2	27.3	373.15	12	768.4	37.0
298.15	14	186.5	26.7	373.15	14	710.5	34.7
298.15	16	169.5	26.1	373.15	16	649.4	33.6
298.15	18	155.0	25.8	373.15	18	589.5	32.6
298.15	20	142.3	25.7	373.15	20	534.8	31.9
298.15	25	115.8	25.0	373.15	25	429.8	30.5
298.15	30	94.6	23.7	373.15	30	358.6	29.1
298.15	35	76.6	22.2	373.15	35	308.0	28.3
298.15	40	61.3	20.8[b]	373.15	40	268.6	27.6
298.15	45	47.7	20.2[c]	373.15	45	237.5	27.2
298.15	50	35.6	19.3[d]	373.15	50	211.0	26.7
323.15	2	1000.5	59.6	423.15	2	935.9	46.3
323.15	4	958.2	51.7	423.15	4	911.0	43.7
323.15	6	902.9	45.0	423.15	6	884.1	41.2
323.15	8	820.0	39.5	423.15	8	855.3	39.2
323.15	10	655.8	36.9	423.15	10	825.0	37.0
323.15	12	456.4	34.8	423.15	12	792.1	34.7
323.15	14	370.0	33.6	423.15	14	758.0	32.4
323.15	16	321.0	33.1	423.15	16	722.7	30.8
323.15	18	286.9	32.8	423.15	18	686.9	29.0
323.15	20	260.6	32.4	423.15	20	651.5	27.5
323.15	25	213.1	31.6	423.15	25	566.1	25.4
323.15	30	178.9	30.6	423.15	30	493.4	23.9
323.15	35	152.6	30.3	423.15	35	432.7	22.7
323.15	40	130.3	29.2	423.15	40	384.3	21.7
323.15	45	112.1	29.1	423.15	45	343.3	21.2
323.15	50	95.4	29.8[b]	423.15	50	310.0	20.9
343.15	2	988.0	58.2	448.15	2	915.4	42.5
343.15	4	952.4	52.4	448.15	4	892.5	40.7
343.15	6	908.7	46.9	448.15	6	868.3	38.6
343.15	8	853.6	42.1	448.15	8	842.8	36.4
343.15	10	780.9	38.5	448.15	10	816.2	34.6
343.15	12	684.1	36.4	448.15	12	788.1	32.0
343.15	14	574.6	34.9	448.15	14	759.3	29.9
343.15	16	484.6	33.5	448.15	16	729.8	28.1
343.15	18	421.1	32.7	448.15	18	699.9	27.3
343.15	20	375.3	32.3	448.15	20	670.4	26.5
343.15	25	299.9	31.3	448.15	25	597.3	24.5
343.15	30	251.1	30.6	448.15	30	531.9	22.5
343.15	35	215.2	30.0	448.15	35	474.0	20.9
343.15	40	186.8	29.7	448.15	40	425.9	20.2
343.15	45	163.3	29.2	448.15	45	383.9	19.4
343.15	50	143.3	29.3	448.15	50	349.3	18.9

[a]Standard uncertainties u are $u(T)$ = 0.025 K, $u(p)$ = 35 kPa, and $u(\gamma)$ = max(0.008γ, 0.3 mN·m^{-1}). [b]$u(\gamma)$ = 0.4 mN·m^{-1}. [c]$u(\gamma)$ = 0.5 mN·m^{-1}. [d]$u(\gamma)$ = 0.6 mN·m^{-1}.

Table 3. Interfacial Tension γ for CO_2 + (0.864 NaCl + 0.136 KCl)(aq) at Temperatures T, Pressures p, and Total Salt Molality m = 1.98 mol·kg^{-1} [a]

T	p	$\Delta\rho$	γ	T	p	$\Delta\rho$	γ
K	MPa	kg·m^{-3}	mN·m^{-1}	K	MPa	kg·m^{-3}	mN·m^{-1}
323.15	2	1031.6	61.0	373.15	18	620.3	34.4
323.15	4	989.3	53.4	373.15	20	565.2	33.5
323.15	6	933.9	46.5	373.15	25	460.1	32.0
323.15	8	850.8	40.0	373.15	30	388.6	30.8
323.15	10	686.5	37.1	373.15	35	337.9	30.1
323.15	12	487.1	35.4	373.15	40	298.1	29.7
323.15	14	400.6	35.0	373.15	45	267.2	29.1
323.15	16	351.6	34.5	373.15	50	240.2	28.4
323.15	18	317.4	33.7	393.15	2	991.7	54.1
323.15	20	290.9	33.4	393.15	4	963.2	50.5
323.15	25	243.4	32.5	393.15	6	931.7	47.0
323.15	30	208.8	31.9	393.15	8	897.0	43.9
323.15	35	182.6	31.9	393.15	10	858.8	40.8
323.15	40	159.9	30.5	393.15	12	817.2	38.5
323.15	45	141.8	30.7	393.15	14	772.3	36.5
323.15	50	124.7	29.8	393.15	16	725.2	35.1
343.15	2	1020.3	59.2	393.15	18	677.5	33.8
343.15	4	984.2	53.3	393.15	20	631.0	32.7
343.15	6	940.2	48.5	393.15	25	529.2	30.7
343.15	8	884.8	43.8	393.15	30	452.0	29.5
343.15	10	811.9	40.2	393.15	35	394.1	28.7
343.15	12	715.0	37.9	393.15	40	349.1	27.9
343.15	14	605.3	36.8	393.15	45	312.8	27.5
343.15	16	515.1	35.6	393.15	50	282.7	27.0
343.15	18	451.6	34.8	423.15	2	970.2	48.9
343.15	20	405.8	34.2	423.15	4	944.8	45.5
343.15	25	330.1	33.1	423.15	6	917.5	43.1
343.15	30	281.2	31.9	423.15	8	888.3	41.1
343.15	35	245.2	31.2	423.15	10	857.9	38.8
343.15	40	216.7	30.9	423.15	12	824.4	36.8
343.15	45	193.1	30.3	423.15	14	790.1	35.0
343.15	50	173.0	29.9	423.15	16	754.5	34.0
373.15	2	1004.4	57.0	423.15	18	718.4	32.0
373.15	4	973.3	52.4	423.15	20	683.3	30.8
373.15	6	938.1	48.3	423.15	25	596.9	28.7
373.15	8	897.9	44.6	423.15	30	524.2	27.4
373.15	10	851.7	41.5	423.15	35	462.7	26.2
373.15	12	799.7	38.9	423.15	40	414.4	25.4
373.15	14	741.6	37.0	423.15	45	372.6	24.8
373.15	16	680.3	35.6	423.15	50	339.5	24.3

[a]Standard uncertainties u are $u(T)$ = 0.025 K, $u(p)$ = 35 kPa, and $u(\gamma)$ = max(0.008γ, 0.3 mN·m^{-1}).

seen that γ decreases rapidly with increasing pressure when the pressure is lower than the critical pressure of CO_2; thereafter γ decreases more gradually with increasing pressure. Figure 6 shows the same data plotted along isobars as a function of temperature, and it can be seen that the trends, while smooth, are more complicated. This has also been noted in the literature.[21,24,38,39]

Thermodynamic expressions for the derivatives γ with respect to temperature and pressure may be obtained from the Gibbs−Duhem equation applied to the surface phase and to the two bulk phases. Since, in the present case, these derivatives are only weakly dependent upon the salt molality, it is sufficient to consider the binary (water + CO_2) system. It is shown in the appendix that, for a system containing two components of low mutual solubility, $-(\partial\gamma/\partial T)_p$ is proportional to the excess molar entropy of the surface phase, while $(\partial\gamma/\partial p)_T$ is proportional to the excess molar volume of the surface phase. Thus the present results give an indication of the sign of these excess properties of the surface phase.

dx.doi.org/10.1021/je201062r | J. Chem. Eng. Data 2012, 57, 1078−1088

Table 4. Interfacial Tension γ for CO_2 + (0.864 NaCl + 0.136 KCl)(aq) at Temperatures T, Pressures p, and Total Salt Molality m = 2.97 mol·kg^{-1} [a]

T	p	$\Delta\rho$	γ	T	p	$\Delta\rho$	γ
K	MPa	kg·m^{-3}	mN·m^{-1}	K	MPa	kg·m^{-3}	mN·m^{-1}
298.15	2	1078.0	62.0	373.15	2	1043.3	58.2
298.15	4	1025.2	51.0	373.15	4	1011.8	53.5
298.15	6	928.7	38.5	373.15	6	976.3	48.7
298.15	8	343.4	35.3	373.15	8	935.9	45.4
298.15	10	303.7	34.7	373.15	10	889.4	42.5
298.15	12	276.2	34.3	373.15	12	837.3	40.3
298.15	14	255.3	34.1	373.15	14	779.1	38.2
298.15	16	238.1	33.9	373.15	16	717.7	36.7
298.15	18	223.3	34.0	373.15	18	657.5	35.2
298.15	20	210.8	34.0	373.15	20	602.2	34.7
298.15	25	183.5	33.2	373.15	25	497.0	33.7
298.15	30	162.2	32.6	373.15	30	425.0	32.3
298.15	35	143.6	31.7	373.15	35	374.5	31.2
298.15	40	128.0	32.3	373.15	40	334.2	30.6
298.15	45	113.8	31.6	373.15	45	303.4	30.1
298.15	50	101.6	30.8	373.15	50	275.9	29.6
323.15	2	1069.2	63.5	393.15	2	1031.1	56.2
323.15	4	1026.8	54.9	393.15	4	1002.2	52.7
323.15	6	971.3	48.0	393.15	6	970.4	49.4
323.15	8	888.2	41.5	393.15	8	935.5	46.2
323.15	10	723.8	38.5	393.15	10	897.1	43.3
323.15	12	524.4	37.7	393.15	12	855.2	40.7
323.15	14	437.8	36.6	393.15	14	810.1	38.7
323.15	16	388.7	35.8	393.15	16	762.9	37.2
323.15	18	354.5	35.8	393.15	18	715.0	35.7
323.15	20	327.8	35.5	393.15	20	668.3	34.6
323.15	25	280.3	34.8	393.15	25	566.3	32.3
323.15	30	245.3	33.5	393.15	30	488.8	30.9
323.15	35	219.2	32.9	393.15	35	430.6	30.3
323.15	40	196.0	32.7	393.15	40	385.4	29.5
323.15	45	178.2	32.1	393.15	45	349.0	28.8
323.15	50	160.5	31.5	393.15	50	318.7	28.3
343.15	2	1058.8	62.2	423.15	2	1010.9	51.6
343.15	4	1022.3	56.7	423.15	4	985.1	48.5
343.15	6	978.0	51.3	423.15	6	957.5	45.8
343.15	8	922.4	43.8	423.15	8	927.9	43.5
343.15	10	849.3	40.8	423.15	10	897.6	41.1
343.15	12	752.3	39.0	423.15	12	863.5	39.1
343.15	14	642.4	37.9	423.15	14	828.8	37.4
343.15	16	552.2	36.6	423.15	16	793.1	35.8
343.15	18	488.6	36.2	423.15	18	756.8	34.4
343.15	20	442.7	35.7	423.15	20	721.8	33.5
343.15	25	366.9	34.8	423.15	25	634.6	31.5
343.15	30	317.9	34.1	423.15	30	562.0	30.1
343.15	35	281.8	33.4	423.15	35	499.6	28.9
343.15	40	253.2	33.0	423.15	40	451.6	28.1
343.15	45	229.5	32.4	423.15	45	408.8	27.3
343.15	50	209.3	32.2	423.15	50	376.2	26.9

[a] Standard uncertainties u are $u(T)$ = 0.025 K, $u(p)$ = 35 kPa, and $u(\gamma)$ = max(0.008γ, 0.3 mN·m^{-1}).

Variation with Salinity. The effect of salinity (both ion type and concentration) on water surface tension under ambient conditions is documented in the literature.[40,41] The present results indicate that the interfacial tension increases with salinity and always exceeds that of salt-free water at the same pressure and temperature. Indeed, our results clearly show that at every temperature and pressure investigate, γ increases *linearly* with the salt concentration. This behavior is exemplified by the results at T = (343.15 and 373.15) K shown in Figures 7 and 8, respectively. Data for zero molality of salt from[20] are also plotted in these figures and fall precisely in line with the linear trends exhibited by our data for finite molality.

At a molecular level, the explanation for the observed behavior is that the ions, being excluded from the CO_2-rich phase, have a negative affinity for the interface and

dx.doi.org/10.1021/je201062r | J. Chem. Eng. Data 2012, 57, 1078–1088

Table 5. Interfacial Tension γ for CO_2 + (0.864 NaCl + 0.136 KCl)(aq) at Temperatures T, Pressures p, and Total Salt Molality m = 4.95 mol·kg^{-1} [a]

T	p	$\Delta\rho$	γ	T	p	$\Delta\rho$	γ
K	MPa	kg·m^{-3}	mN·m^{-1}	K	MPa	kg·m^{-3}	mN·m^{-1}
323.15	2	1117.5	65.8	373.15	2	1092.8	61.3
323.15	4	1075.0	57.2	373.15	4	1061.0	57.8
323.15	6	1019.4	50.7	373.15	6	1025.1	53.2
323.15	8	936.2	44.8	373.15	8	984.5	49.4
323.15	10	771.6	41.8	373.15	10	937.6	46.1
323.15	12	572.2	40.1	373.15	12	885.5	43.9
323.15	14	485.5	39.3	373.15	14	827.1	42.1
323.15	16	436.4	38.9	373.15	16	765.6	40.6
323.15	18	402.1	38.4	373.15	18	705.2	39.5
323.15	20	375.2	38.0	373.15	20	649.5	38.0
323.15	25	327.7	37.0	373.15	25	544.4	36.7
323.15	30	292.2	36.6	373.15	30	471.8	35.3
323.15	35	266.3	36.2	373.15	35	421.4	34.8
323.15	40	242.5	35.6	373.15	40	380.6	34.2
323.15	45	225.1	35.4	373.15	45	350.1	33.8
323.15	50	206.6	34.7	373.15	50	321.9	33.2
343.15	2	1107.9	64.9	423.15	2	1062.8	55.7
343.15	4	1070.9	58.6	423.15	4	1036.5	52.4
343.15	6	1026.3	52.9	423.15	6	1008.5	49.8
343.15	8	970.5	47.7	423.15	8	978.6	46.8
343.15	10	897.3	44.3	423.15	10	948.3	44.3
343.15	12	800.1	42.3	423.15	12	913.4	42.6
343.15	14	690.1	40.8	423.15	14	878.5	40.9
343.15	16	599.8	39.7	423.15	16	842.5	39.6
343.15	18	536.1	38.8	423.15	18	805.9	38.2
343.15	20	490.1	38.3	423.15	20	771.3	37.4
343.15	25	414.2	37.2	423.15	25	683.0	35.3
343.15	30	365.0	36.3	423.15	30	610.6	34.0
343.15	35	328.8	35.5	423.15	35	547.1	32.8
343.15	40	300.1	34.8	423.15	40	499.5	31.9
343.15	45	276.3	34.3	423.15	45	455.7	31.5
343.15	50	256.0	33.5	423.15	50	423.6	31.0

[a] Standard uncertainties u are $u(T)$ = 0.025 K, $u(p)$ = 35 kPa, and $u(\gamma)$ = max(0.008γ, 0.3 mN·m^{-1}).

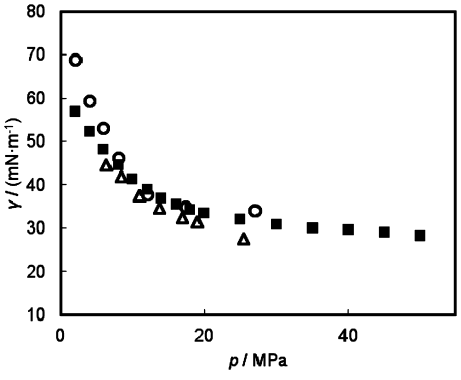

Figure 4. Interfacial tension of CO_2 + (0.864 NaCl + 0.136 KCl)(aq) as a function of pressure at T = 373 K: ■, this work, m = 1.98 mol·kg^{-1}; ○, Bachu and Bennion,[18] m = 2.15 mol·kg^{-1}; △, Chalbaud et al.,[17] m = 1.79 mol·kg^{-1}.

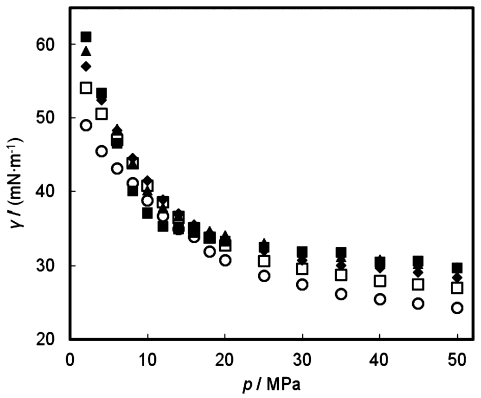

Figure 5. Interfacial tension of CO_2 + (0.864 NaCl + 0.136 KCl)(aq), m = 1.98 mol·kg^{-1}, as a function of pressure at different isotherms: ■, T = 323.15 K; ▲, T = 343.15 K; □, T = 393.15 K; ○, T = 423.15 K; ◆, T = 373.15 K.

are restricted to the bulk of the aqueous phase. The resulting gradient in ionic strength near the interface leads to an enhanced attraction of the water molecules toward the bulk of the aqueous phase, thereby increasing the work required to expand the interfacial area and amplifying γ. This effect is expected to increase with both ion concentration and ion charge.

Empirical Equation. For practical purposes, it is useful to have an empirical equation to describe the variation of γ with temperature, pressure, and salinity. From the discussion above,

dx.doi.org/10.1021/je201062r | J. Chem. Eng. Data 2012, 57, 1078–1088

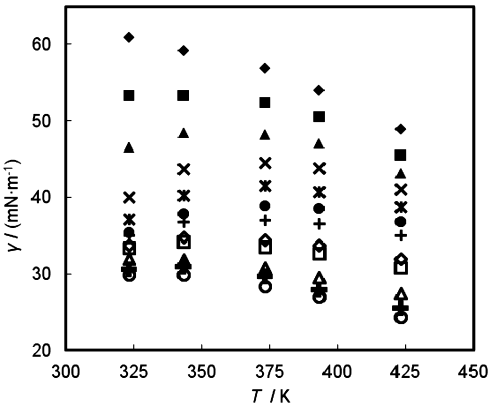

Figure 6. Interfacial tension of CO_2 + (0.864 NaCl + 0.136 KCl)(aq), m = 1.98 mol·kg^{-1}, as a function of temperature at different pressures: ◆, p = 2 MPa; ■, p = 4 MPa; ▲, p = 6 MPa; ×, p = 8 MPa; ∗, p = 10 MPa; ●, p = 12 MPa; +, p = 14 MPa; ◇, p = 18 MPa; □, p = 20 MPa; △, p = 30 MPa; +, p = 40 MPa; ○, p = 50 MPa.

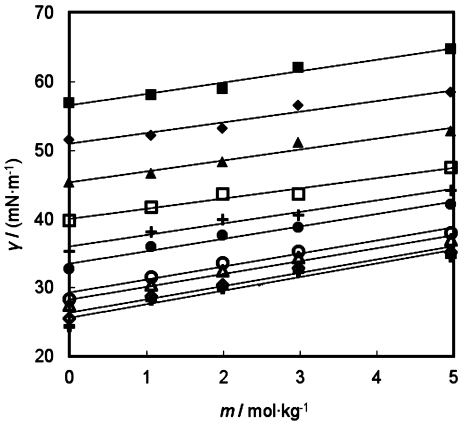

Figure 7. Interfacial tension of CO_2 + (0.864 NaCl + 0.136 KCl)(aq), as a function of salinity, at T = 343.15·K: ■, p = 2 MPa; ◆, p = 4 MPa; ▲, p = 6 MPa; □, p = 8 MPa; +, p = 10 MPa; ●, p = 12 MPa; ○, p = 20 MPa; △, p = 25 MPa; ◇, p = 35 MPa; +, p = 40 MPa. Solid lines are linear fits to the data.

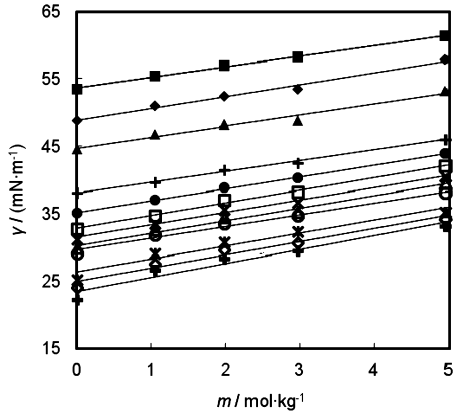

Figure 8. Interfacial tension of CO_2 + (0.864 NaCl + 0.136 KCl)(aq), as a function of salinity, at T = 373.15 K: ■, p = 2 MPa; ◆, p = 4 MPa; ▲, p = 6 MPa; +, p = 10 MPa; ●, p = 12 MPa; □, p = 14 MPa; ×, p = 16 MPa; △, p = 18 MPa; ○, p = 20 MPa; ∗, p = 30 MPa; ◇, p = 40 MPa; +, p = 50 MPa. Solid lines are linear fits to the data.

it is clear that the present results can be correlated as a linear function of molality as follows:

$$\gamma/(\mathrm{mN\cdot m^{-1}}) = A[m/(\mathrm{mol\cdot kg^{-1}})] + B \quad (7)$$

Here A and B are functions of temperature and pressure, the latter representing $\gamma/(\mathrm{mol\cdot kg^{-1}})$ for the (CO_2 + H_2O) system. Considering all of the data at $T \geq 323.15$ K, the following expressions, containing in total 12 parameters, were obtained

$$A = a_0 + a_1(p/\mathrm{MPa}) + a_2(T/\mathrm{K}) \quad (8)$$

$$B = [b_{00} + b_{01}(T/\mathrm{K}) + b_{02}(T/\mathrm{K})^2] + [b_{10} + b_{11}(T/\mathrm{K})](p/\mathrm{MPa})^{-1} + [b_{20} + b_{21}(T/\mathrm{K})](p/\mathrm{MPa})^{-2} + [b_{30} + b_{31}(T/\mathrm{K})](p/\mathrm{MPa})^{-3} \quad (9)$$

The parameters appearing in eqs 8 and 9 are given in Table 6, and relative deviations of the experimental data are shown in

Table 6. Parameters in Equations 8 and 9 for the Correlation of the Interfacial Tension of CO_2 + (0.864 NaCl + 0.136 KCl)(aq)

a_0	0.451012	b_{10}	−538.898050
a_1	0.006202	b_{11}	2.030519
a_2	0.003365	b_{20}	3831.239088
b_{00}	−41.203583	b_{21}	−11.694413
b_{01}	0.435486	b_{30}	−5165.927448
b_{02}	−0.000725	b_{31}	15.072621

Figure 9. The expanded uncertainty of this correlation is 1.6 mN·m^{-1} with a coverage factor k = 2, and the vast majority of

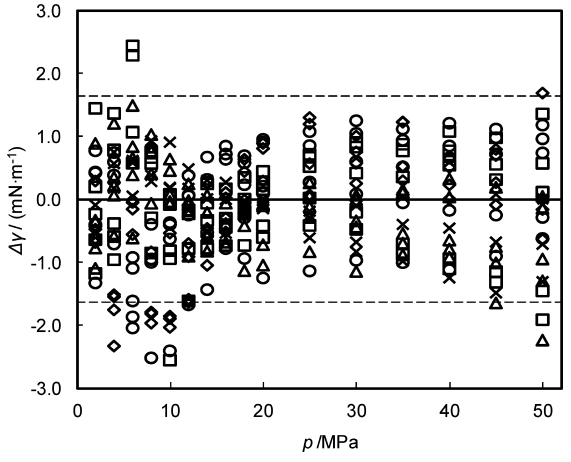

Figure 9. Deviation $\Delta\gamma$ of the interfacial tension of CO_2 + (0.864 NaCl + 0.136 KCl)(aq) from eq 7: ◇, T = 323.15 K; □, T = 343.15·K; △, T = 373.15 K; ×, T = 393.15 K; ○, T = 423.15 K. Dashed lines show the uncertainty bounds of the correlation with a coverage factor k = 2.

the data are fitted to within 1 mN·m^{-1}. Nevertheless, a few points exhibit larger, mostly negative, deviations that could not be reduced without adding many additional parameters.

CONCLUSIONS

A new apparatus for measuring interfacial tension γ at high pressures has been constructed and used to measure γ for the

dx.doi.org/10.1021/je201062r | J. Chem. Eng. Data 2012, 57, 1078−1088

CO_2 + (0.864 NaCl + 0.136 KCl)(aq) system over wide ranges of temperature, pressure, and molality. The results clearly demonstrate a linear dependence of γ on molality over the whole range investigated, and a simple empirical equation was used to correlate the data.

APPENDIX

The variation of interfacial tension with temperature and pressure may be deduced following Guggenheim's analysis[42] in which the interfacial region is treated as a microphase of small but finite thickness. The Gibbs−Duhem equation applied to this surface phase in a two-component system with a planar interface is:

$$-Ad\gamma = S^{\sigma}dT - V^{\sigma}dp + n_1^{\sigma}d\mu_1 + n_2^{\sigma}d\mu_2 \quad \text{(A1)}$$

Here, A is the area of the interface, S denotes entropy, V is volume, n_i is the amount of component i, μ_i is the chemical potential of component i, and superscript σ denotes properties of the surface phase. Similarly, for the two bulk phases, denoted α and β, we have:

$$0 = S^{\alpha}dT - V^{\alpha}dp + n_1^{\alpha}d\mu_1 + n_2^{\alpha}d\mu_2 \quad \text{(A2)}$$

and

$$0 = S^{\beta}dT - V^{\beta}dp + n_1^{\beta}d\mu_1 + n_2^{\beta}d\mu_2 \quad \text{(A3)}$$

Combining these equations at constant pressure to eliminate of the chemical potentials, one finds:

$$-Ad\gamma = n^{\sigma}[S_m^{\sigma} - [(z_1(y_2S_m^{\alpha} - x_2S_m^{\beta}) + z_2(x_1S_m^{\beta} - y_1S_m^{\alpha}))/(x_1y_2 - y_1x_2)]]dT \quad \text{(A4)}$$

where x_i, y_i, and z_i denote mole fractions of component i in phases α, β, and σ, respectively, subscript m denotes molar properties, and n^{σ} is the total amount of substance in the surface phase. When the two components are only sparingly soluble in each other, we have (assuming α to be the phase rich in component 1) $x_1 \approx y_2 \approx 1$ and hence $x_2 \approx 0$ and $y_1 \approx 0$ so that

$$(\partial\gamma/\partial T)_p = -(n^{\sigma}/A)(S_m^{\sigma} - z_1S_1 - z_2S_2) \quad \text{(A5)}$$

where S_1 and S_2 are the molar entropies of the pure components 1 and 2 at the temperature and pressure of the system. Similarly, for the variation with pressure, one finds

$$(\partial\gamma/\partial p)_T = (n^{\sigma}/A)(V_m^{\sigma} - z_1V_1 - z_2V_2) \quad \text{(A6)}$$

where V_1 and V_2 are the molar volume of the pure components 1 and 2. Thus, $-(\partial\gamma/\partial T)_p$ is proportional to the excess molar entropy of the surface phase, while $(\partial\gamma/\partial p)_T$ is proportional to the excess molar volume of the surface phase.

AUTHOR INFORMATION

Corresponding Author

*E-mail: m.trusler@imperial.ac.uk.

Funding

This work was carried out as part of the activities of the Qatar Carbonates and Carbon Storage Research Centre (QCCSRC). We gratefully acknowledge the funding of QCCSRC provided jointly by Qatar Petroleum, Shell, and the Qatar Science and Technology Park, and their permission to publish this research.

Notes

The authors declare no competing financial interest.

REFERENCES

(1) Shedid, A. S. Influences of fracture orientation on oil recovery by water and polymer flooding processes: An experimental approach. *J. Pet. Sci. Eng.* **2006**, *50*, 285−292.

(2) Blunt, M.; Fayers, F. J.; Orr, F. M., Jr. Carbon dioxide in enhanced oil recovery. *Energy Convers. Manage.* **1993**, *34*, 1197−1204.

(3) Rogers, J. D.; Grigg, R. B. A literature analysis of the WAG injectivity abnormalities in the CO_2 process. *SPE Reservoir Eval. Eng.* **2001**, *4*, 375−386.

(4) Blom, S. M. P.; Hagoort, J.; Soetekouw, D. P. N. Relative permeability at near-critical conditions. *SPE J.* **2000**, *5*, 172−181.

(5) Blom, S. M. P.; Hagoort, J. The combined effect of near-critical relative permeability and non-Darcy flow on well impairment by condensate drop out. *SPE Reservoir Eval. Eng.* **1998**, *1*, 421−429.

(6) Grattoni, C. A.; Jing, X. D.; Dawe, R. A. Dimensionless groups for three-phase gravity drainage flow in porous media. *J. Pet. Sci. Eng.* **2001**, *29*, 53−65.

(7) Bennion, D. B.; Bachu, S. The Impact of Interfacial Tension and Pore Size Distribution/Capillary Pressure Character on CO_2 Relative Permeability at Reservoir Conditions in CO_2-Brine Systems. In *SPE/DOE Symposium on Improved Oil Recovery*, Tulsa, OK, 2006.

(8) Bachu, S.; Bennion, B. Effects of in-situ conditions on relative permeability characteristics of CO_2-brine systems. *Environ. Geol.* **2008**, *54*, 1707−1722.

(9) Jaeger, P. T.; Alotaibi, M. B.; Nasr-El-Din, H. A. Influence of Compressed Carbon Dioxide on the Capillarity of the Gas−Crude Oil−Reservoir Water System. *J. Chem. Eng. Data* **2010**, *55*, 5246−5251.

(10) Karimaie, H.; Torsæter, O. Low IFT gas-oil gravity drainage in fractured carbonate porous media. *J. Pet. Sci. Eng.* **2010**, *70*, 67−73.

(11) Sun, C.-Y.; Chen, G.-J. Measurement of Interfacial Tension for the CO_2 Injected Crude Oil + Reservoir Water System. *J. Chem. Eng. Data* **2005**, *50*, 936−938.

(12) Yang, D. Y.; Tontiwachwuthikul, P.; Gu, Y. G. Dynamic interfacial tension method for measuring gas diffusion coefficient and interface mass transfer coefficient in a liquid. *Ind. Eng. Chem. Res.* **2006**, *45*, 4999−5008.

(13) Yang, D.; Tontiwachwuthikul, P.; Gu, Y. Interfacial Tensions of the Crude Oil + Reservoir Brine + CO_2 Systems at Pressures up to 31 MPa and Temperatures of 27 and 58 °C. *J. Chem. Eng. Data* **2005**, *50*, 1242−1249.

(14) Jarrell, P. M.; Fox, C. E.; Stein, M. H.; Webb, S. L. *Practical Aspects of CO_2 flooding*; Society of Petroleum Engineers: Dallas, TX, 2002; Vol. 22.

(15) Morozova, D.; Wandrey, M.; Alawi, M.; Zimmer, M.; Vieth, A.; Zettlitzer, M.; Würdemann, H. Monitoring of the microbial community composition in saline aquifers during CO_2 storage by fluorescence in situ hybridisation. *Int. J. Greenhouse Gas Control* **2010**, *4*, 981−989.

(16) Metz, B.; Davidson, O.; Bosch, P.; Dave, R.; Meyer, L. *Climate change 2007 - mitigation of climate change*; Cambridge University Press: Cambridge, U.K., 2007; p 896.

(17) Chalbaud, C.; Robin, M.; Lombard, J. M.; Martin, F.; Egermann, P.; Bertin, H. Interfacial tension measurements and wettability evaluation for geological CO_2 storage. *Adv. Water Res.* **2009**, *32*, 98−109.

(18) Bachu, S.; Bennion, D. B. Interfacial Tension between CO_2, Freshwater, and Brine in the Range of Pressure from (2 to 27) MPa, Temperature from (20 to 125) °C, and Water Salinity from (0 to 334 000) mg·L^{-1}. *J. Chem. Eng. Data* **2009**, *54*, 765−775.

(19) Chiquet, P.; Daridon, J. L.; Broseta, D.; Thibeau, S. CO_2/water interfacial tensions under pressure and temperature conditions of CO_2 geological storage. *Energy Convers. Manage.* **2007**, *48*, 736−744.

(20) Georgiadis, A.; Maitland, G.; Trusler, J. P. M.; Bismarck, A. Interfacial Tension Measurements of the (H_2O + CO_2) System at

Elevated Pressures and Temperatures. *J. Chem. Eng. Data* **2010**, *55*, 4168−4175.
(21) Bachu, S.; Bennion, D. B. Dependence of CO_2-brine interfacial tension on aquifer pressure, temperature and water salinity. In *9th International Conference on Greenhouse Gas Control Technologies*; Gale, J., Herzog, H., Braitsch, J., Eds.; Elsevier Science BV: Washington, DC, 2009; Vol. *1*, pp 3157−3164.
(22) Yang, D. Y.; Tontiwachwuthikul, P.; Gu, Y. G. Interfacial interactions between reservoir brine and CO_2 at high pressures and elevated temperatures. *Energy Fuels* **2005**, *19*, 216−223.
(23) Aggelopoulos, C. A.; Robin, M.; Perfetti, E.; Vizika, O. CO_2/$CaCl_2$ solution interfacial tensions under CO_2 geological storage conditions: Influence of cation valence on interfacial tension. *Adv. Water Res.* **2010**, *33*, 691−697.
(24) Aggelopoulos, C. A.; Robin, M.; Vizika, O. Interfacial tension between CO_2 and brine (NaCl + $CaCl_2$) at elevated pressures and temperatures: The additive effect of different salts. *Adv. Water Res.*, in press.
(25) Hansen, F. K. Surface Tension by Image Analysis: Fast and Automatic Measurements of Pendant and Sessile Drops and Bubbles. *J. Colloid Interface Sci.* **1993**, *160*, 209−217.
(26) Hansen, F. K.; Rødsrud, G. Surface tension by pendant drop: I. A fast standard instrument using computer image analysis. *J. Colloid Interface Sci.* **1991**, *141*, 1−9.
(27) Fordham, S. On the Calculation of Surface Tension from Measurements of Pendant Drops. *Proc. R. Soc. London, A* **1948**, *194*, 1−16.
(28) Hull, T. E.; Enright, W. H.; Jackson, K. R. Runge-Kutta research at Toronto. *Appl. Numer. Math.* **1996**, *22*, 225−236.
(29) Hebach, A.; Oberhof, A.; Dahmen, N. Density of Water + Carbon Dioxide at Elevated Pressures: Measurements and Correlation. *J. Chem. Eng. Data* **2004**, *49*, 950−953.
(30) Duan, Z. H.; Sun, R.; Zhu, C.; Chou, I. M. An improved model for the calculation of CO_2 solubility in aqueous solutions containing Na^+, K^+, Ca^{2+}, Mg^{2+}, Cl^-, and SO_4^{2-}. *Mar. Chem.* **2006**, *98*, 131−139.
(31) Pruess, K.; Spycher, N. ECO2N - A fluid property module for the TOUGH2 code for studies of CO_2 storage in saline aquifers. *Energy Convers. Manage.* **2007**, *48*, 1761−1767.
(32) Al Ghafri, S.; Maitland, G. C.; Trusler, J. P. M. Densities of aqueous $MgCl_2$(aq), $CaCl_2$(aq), KI(aq), NaCl(aq), KCl(aq), $AlCl_3$(aq) and (0.964 NaCl + 0.136 KCl)(aq) at temperatures between (283 and 472) K, pressures up to 68.5 MPa and molalities up to 6 mol·kg^{-1}. *J. Chem. Eng. Data*, submitted.
(33) Span, R.; Wagner, W. A new equation of state for carbon dioxide covering the fluid region from the triple-point temperature to 1100 K at pressures up to 800 MPa. *J. Phys. Chem. Ref. Data* **1996**, *25*, 1509−1596.
(34) da Rocha, S. R. P.; Harrison, K. L.; Johnston, K. P. Effect of Surfactants on the Interfacial Tension and Emulsion Formation between Water and Carbon Dioxide. *Langmuir* **1998**, *15*, 419−428.
(35) Hebach, A.; Oberhof, A.; Dahmen, N.; Kögel, A.; Ederer, H.; Dinjus, E. Interfacial Tension at Elevated Pressures Measurements and Correlations in the Water + Carbon Dioxide System. *J. Chem. Eng. Data* **2002**, *47*, 1540−1546.
(36) Tewes, F.; Boury, F. Thermodynamic and Dynamic Interfacial Properties of Binary Carbon Dioxide−Water Systems. *J. Phys. Chem. B* **2004**, *108*, 2405−2412.
(37) Pallas, N. R.; Harrison, Y. An automated drop shape apparatus and the surface tension of pure water. *Colloids Surf.* **1990**, *43*, 169−194.
(38) Chalbaud, C.; Robin, M.; Lombard, J. M.; Bertin, H.; Egermann, P. Brine/CO_2 Interfacial Properties and Effects on CO_2 Storage in Deep Saline Aquifers. *Oil Gas Sci. Technol.* **2010**, *65*, 541−555.
(39) Yang, D. Y.; Tontiwachwuthikul, P.; Gu, Y. G. Interfacial tensions of the crude oil plus reservoir brine + CO_2 systems at pressures up to 31 MPa and temperatures of 27 °C and 58 °C. *J. Chem. Eng. Data* **2005**, *50*, 1242−1249.
(40) Johansson, K.; Eriksson, J. C. γ and dγ/dT measurements on aqueous solutions of 1,1-electrolytes. *J. Colloid Interface Sci.* **1974**, *49*, 469−480.
(41) Ali, K.; Anwar-ul-Haq; Bilal, S.; Siddiqi, S. Concentration and temperature dependence of surface parameters of some aqueous salt solutions. *Colloids Surf., A* **2006**, *272*, 105−110.
(42) Guggenheim, E. A. The thermodynamics of interfaces in systems of several components. *Trans. Faraday Soc.* **1940**, *36*, 397−412.